 CMES, vol.94, no.4, pp.331-369, 2013

GDQFEM Numerical Simulations of Continuous Media with Cracks and Discontinuities

E. Viola[1], F. Tornabene[1] E. Ferretti[1] and N. Fantuzzi[1]

Abstract: In the present paper the Generalized Differential Quadrature Finite Element Method (GDQFEM) is applied to deal with the static analysis of plane state structures with generic through the thickness material discontinuities and holes of various shapes. The GDQFEM numerical technique is an extension of the Generalized Differential Quadrature (GDQ) method and is based on the idea of conventional integral quadrature. In particular, the GDQFEM results in terms of stresses and displacements for classical and advanced plane stress problems with discontinuities are compared to the ones by the Cell Method (CM) and Finite Element Method (FEM). The multi-domain technique is implemented in a MATLAB code for solving irregular domains with holes and defects. In order to demonstrate the accuracy of the proposed methodology, several numerical examples of stress and displacement distributions are graphically shown and discussed.

Keywords: Generalized Differential Quadrature Finite Element Method, Cracks and Discontinuities, Cell Method.

1 Introduction

Dealing with elastic structures containing cracks and material discontinuities has always been a complicated problem to solve numerically, due to high-order gradients of the solutions in terms of displacements and stresses at crack tips and edges [Li, Shen, Han, and Atluri (2003); Sladek, Sladek, and Atluri (2004); Viola and Marzani (2004); Viola, Artioli, and Dilena (2005); Han, Liu, Rajendran, and Atluri (2006); Ricci and Viola (2006); Viola, Ricci, and Aliabadi (2007); Li and Atluri (2008a,b)]. Computational problems are connected with the numerical techniques under consideration. For instance, the well-known Finite Element Method (FEM) has a lot of numerical issues when line cracks and holes are present in physical models. For this reason many scientists have tried new ways for analysing elastic structures using alternative numerical techniques [Viola, Li, and Fantuzzi (2012);

[1] DICAM Department, University of Bologna, Italy.

Viola, Fantuzzi, and Marzani (2012); Li and Viola (2013); Li, Fantuzzi, and Tornabene (2013)]. However, in this work it is assumed that there is no contact between two separated parts of a body and the singularity effects at the crack tip or at the ends of material discontinuities are not investigated. The same assumption was considered by other researchers in recent papers [Huang, Leissa, and Liao (2008); Huang and Leissa (2009); Huang, Leissa, and Chan (2011); Huang, Leissa, and Li (2011)] when fracture mechanics is not the main purpose of the study, such as the one presented in this paper. In addition, concerning the materials and the loads considered in this paper, the plastic zone is very small with respect to the crack dimensions. Thus, the crack can be considered equal to the initial crack length, due to the fact that it does not propagate. In a future study, the fracture mechanics analysis according to the approach outlined in the papers [Dong and Atluri (2012, 2013a,b)] will be taken into account. Here, the Generalized Differential Quadrature Finite Element Method (GDQFEM) is investigated, nevertheless any special element is considered for treating the singularity connected with fracture mechanics problems. In fact, any kind of discontinuity is treated as a free edge boundary. There are some other methods which differ from FEM that can deal with cracks and discontinuities, too. In particular, the Cell Method (CM) [Tonti (2001); Ferretti (2001, 2003, 2004a,b,c, 2005, 2009, 2012); Ferretti, Casadio, and Di Leo (2008)]. The works by [Ferretti (2014, 2013a,b)] are also used in the following.

The main aim of this paper is to compare the numerical solutions obtained through GDQFEM, FEM and CM. The advantages and disadvantages of each method are pointed out. The GDQFEM is an advanced version of the Generalized Differential Quadrature (GDQ) method, which has been applied by the authors to composite plates and shells over the years [Artioli, Gould, and Viola (2005); Viola and Tornabene (2005, 2006, 2009); Tornabene, Fantuzzi, Viola, and Ferreira (2013)]. It should be mentioned that irregular GDQ implementation [Civan and Sliepcevich (1985); Lam (1993); Bert and Malik (1996)] has been introduced in order to solve structures that do not have a regular shape. This occurs in civil, mechanical and aerospace engineering applications, as well as in other fields of science. One of the main advantages of GDQ is linked to its mesh-less behaviour, which is based on the strong formulation of any mathematical problem. Furthermore, it can lead to accurate and reliable results, also using a very small amount of grid points. However, for the classic GDQ application, a regular physical geometry is required, that is the one described by orthogonal Cartesian or curvilinear coordinates [Tornabene (2009, 2011b,a,c)]. In the present work, the geometrical and material discontinuities are treated by dividing the whole physical domain into several sub-domains. The GDQFEM mesh should follow the irregularities of the problem under consideration. Nevertheless, for every sub-domain the mechanical and geometric proper-

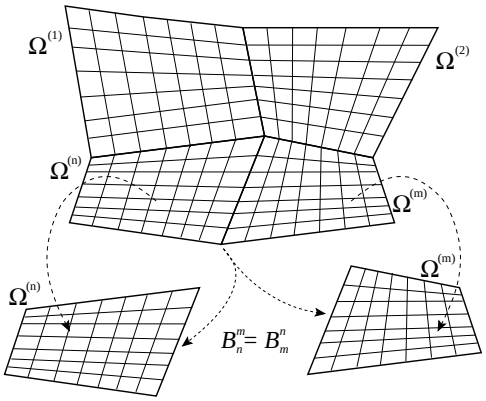

Figure 1: Generic irregular domain configuration and sub-domain decomposition.

ties must be at least continuous. For 2D plane problems these parameters are the thickness and the elastic constants.

2 Plane elasticity equations

As far as plane elastic problems with material discontinuities and holes are concerned, in this paper the basic mathematical formulation is related to two- dimensional elasticity. Thus, the general 2D plane elastic theory is summarized following the book by [Timoshenko (1934)]. The main hypothesis of a 2D plane strain problem concerns the strain components which are $\varepsilon_z = \gamma_{xz} = \gamma_{yz} = 0$. When a plane stress problem is taken into account the out-of-plane stresses are negligible $\sigma_z = \tau_{xz} = \tau_{yz} = 0$. It should be noted that a plane strain state does not correspond to a plane stress one, since $\sigma_z \neq 0$. Analogously, when a plane stress is considered results $\varepsilon_z \neq 0$ and the deformation problem is not plane. The very well-known elastic kinematic relationships, valid both for the plane stress and strain cases, assume the aspect

$$\boldsymbol{\varepsilon} = \mathbf{D}\mathbf{u}, \text{ where } \mathbf{D} = \begin{bmatrix} \frac{\partial}{\partial x} & 0 & \frac{\partial}{\partial y} \\ 0 & \frac{\partial}{\partial y} & \frac{\partial}{\partial x} \end{bmatrix}^T \tag{1}$$

where $\mathbf{D}$ is the kinematic operator, and the strain vector and the displacement vector are defined as $\boldsymbol{\varepsilon} = \begin{bmatrix} \varepsilon_x & \varepsilon_y & \gamma_{xy} \end{bmatrix}^T$, $\mathbf{u} = \begin{bmatrix} u & v \end{bmatrix}^T$, respectively. The constitutive equations, connecting the states of stress and strain, in concise form are

$$\boldsymbol{\sigma} = \mathbf{C}\boldsymbol{\varepsilon}, \text{ where } \mathbf{C} = \begin{bmatrix} 2G+\lambda & \lambda & 0 \\ \lambda & 2G+\lambda & 0 \\ 0 & 0 & G \end{bmatrix} \tag{2}$$

and the stress vector is $\boldsymbol{\sigma} = \begin{bmatrix}\sigma_x & \sigma_y & \tau_{xy}\end{bmatrix}^T$. In all the numerical examples, the Young's modulus E and Poisson's ratio ν are used in place of the Lamè's elastic constants λ and G [Timoshenko (1934)]. The equilibrium equations are reported in compact matrix form

$$\mathbf{D}^*\boldsymbol{\sigma} + \mathbf{f} = \mathbf{0}, \text{ where } \mathbf{D}^* = \begin{bmatrix}\frac{\partial}{\partial x} & 0 & \frac{\partial}{\partial y} \\ 0 & \frac{\partial}{\partial y} & \frac{\partial}{\partial x}\end{bmatrix} \tag{3}$$

and the force vector, which identifies the body forces, is defined by $\mathbf{f} = \begin{bmatrix}f_x & f_y\end{bmatrix}^T$. Since the strong form of the differential problem has to be solved, the fundamental system of equations in terms of displacements parameters u and v must be found. Substituting the kinematic equations in the constitutive ones and the results in the equilibrium equations, the fundamental system for the static case becomes

$$\mathbf{L}\mathbf{u} + \mathbf{f} = \mathbf{0} \tag{4}$$

where $\mathbf{L} = \mathbf{D}^*\mathbf{C}\mathbf{D}$ is named the fundamental operator. The formulation for dynamic plane problems can be obtained from Eq. 4, by adding the inertia forces

$$\mathbf{L}\mathbf{u} + \mathbf{f} = \mathbf{f}_I \tag{5}$$

In Eq. 5 $\mathbf{f}_I = \begin{bmatrix}\rho\ddot{u} & \rho\ddot{v}\end{bmatrix}^T$, ρ denotes the material density and $\ddot{u}$, $\ddot{v}$ stand for the translational accelerations. As it is well-known, the partial differential system of equations Eq. 5 can be only solved when the boundary conditions are included. In the 2D elasticity problems in hand, two types of boundary conditions are enforced: a condition on the displacements $\mathbf{u} = \bar{\mathbf{u}}$ and another condition on the derivatives of the displacement parameters $\frac{\partial \mathbf{u}}{\partial \mathbf{n}} = \mathbf{q}$. The first condition on the displacements is called the kinematic boundary condition or Dirichlet type boundary condition. The second condition on the displacements derivatives is called static boundary condition or Neumann type boundary condition. In particular, for a fixed edge $\bar{\mathbf{u}} = \mathbf{0}$ the vector $\mathbf{q}$ is called the flux vector and in the present paper can be given by the external applied loads to the fixed physical domain, such as normal and shear forces. Since GDQFEM operates on sub-domains, the elements connectivity must be introduced. In the present case the $\mathscr{C}^1$ continuity conditions are enforced. In using the GDQFEM, a domain can have any shape. Using a mapping technique, it is transformed into a set of regular Cartesian parent elements. Thus, the external flux boundary conditions must be written following the outward unit normal vector $\mathbf{n}$ as reported in [Xing, Liu, and Liu (2010); Zhong and He (1998); Zhong and Yu (2009)]

$$\boldsymbol{\sigma}_{\mathbf{n}} = \mathbf{N}\boldsymbol{\sigma}, \text{ where } \mathbf{N} = \begin{bmatrix} n_x^2 & n_y^2 & 2n_x n_y \\ -n_x n_y & n_x n_y & n_x^2 - n_y^2\end{bmatrix} \tag{6}$$

and n_x, n_y are the components of the unit normal vector $\mathbf{n}$, also termed direction cosines. For the sake of completeness, the theoretical development of GDQFEM is explained in the following, in order to show the implementation procedure for the current methodology.

3 Generalized differential quadrature finite element method

As it is well-known from literature [Chen (1999a,b, 2003); Fantuzzi (2013)], the GDQFEM decomposes a domain Ω into several sub-domains or elements $\Omega^{(n)}$, for $n = 1,\ldots,n_e$, where n_e is the total number of sub-domains of the current mesh. A sample of the GDQFEM mesh is depicted in Fig. 1, where four sub-domains are indicated and the external and internal boundary conditions are also underlined. It is important to note that all the couples of sub-domains are considered as disjoint, such as $\Omega^{(n)} \cap \Omega^{(m)} = \emptyset$, for $n \neq m$. The symbol $\emptyset$ is referred to as the empty set. Moreover, the whole physical domain Ω is obtained as $\Omega = \Omega^{(1)} \cup \cdots \cup \Omega^{(n_e)}$, namely the union of a collection of sets. For 2D plane problems, the total degrees of freedom per node are related to the number of constrains. The mathematical problem is regulated by two in-plane displacement parameters u, v. Two boundary conditions per node are involved at the domain external boundary. As a result, the total number of degrees of freedom for any of the following problems can be computed as $N \cdot N \cdot n_e \cdot n_d$, where N are the number of collocation points on a single edge and $n_d = 2$ for 2D plane problems. The inter-element compatibility conditions are enforced by the connection between two adjacent elements, concisely indicated by $B_n^m = B_m^n$. B indicates one of the two conditions that can be imposed for each element edge. The subscripts and superscripts n, m are referred to the two adjacent elements. Indeed the two conditions are algebraically different as it is illustrated in the following. The compatibility, or continuity, conditions between elements entail kinematic and static conditions. These conditions, with reference to Fig. 1, can be indicated as

$$\begin{aligned} &\mathbf{u}^{(n)} = \mathbf{u}^{(m)} \text{ kinematic condition} \\ &\boldsymbol{\sigma}_{\mathbf{n}}^{(n)} = \boldsymbol{\sigma}_{\mathbf{n}}^{(m)} \text{ static condition} \end{aligned} \tag{7}$$

For instance, the kinematic condition is imposed on the left edge that belongs to element $\Omega^{(n)}$ and the static condition is enforced on the right edge that belongs to $\Omega^{(m)}$. In particular the kinematic conditions can be imposed directly, nevertheless the static ones, since they are functions of the outward unit normal vector $\mathbf{n} = \begin{bmatrix} n_x & n_y \end{bmatrix}^T$, follow relation 6. For example, when the kinematic condition is concerned B_n^m indicates the boundary displacements of element $\Omega^{(n)}$ and B_m^n reports the boundary displacements of element $\Omega^{(m)}$. At the same time regarding the

static condition B_n^m contains the stresses $\boldsymbol{\sigma}_{\mathbf{n}}^{(n)}$ of element $\Omega^{(n)}$ that act towards element $\Omega^{(m)}$ and B_m^n, vice versa, are the stresses $\boldsymbol{\sigma}_{\mathbf{n}}^{(m)}$ of element $\Omega^{(m)}$ that correspond to element $\Omega^{(n)}$. Due to the form of the continuity conditions the inter-element accuracy is of $\mathscr{C}^1$ type. Therefore it is higher than the connectivity of standard FEM procedure. In addition to the element edge conditions, the corner type boundary conditions must be considered. The implementation of the corner type boundary conditions for higher-order numerical schemes is still an open problem. In fact very few papers hitherto have been published about this topic [Wang, Wang, and Chen (1998); Wang, Wang, and Zhou (2004); Viola, Tornabene, and Fantuzzi (2013b)]. In the present paper, where the corner belongs to two adjacent elements, the same continuity conditions of the facing sides can be used. When more than two elements share a single corner point a problem arises, since more than two algebraic conditions have to be enforced. For the sake of conciseness, the reference for the actual corner points boundary conditions is the work by [Viola, Tornabene, and Fantuzzi (2013b)]. The numerical integration upon each element is performed through GDQ [Marzani, Tornabene, and Viola (2008); Tornabene and Ceruti (2013a,b)]. However, the GDQ method can be applied only to regular coordinate systems, such as Cartesian or orthogonal curvilinear coordinates [Tornabene, Fantuzzi, Viola, and Reddy (2014); Tornabene, Fantuzzi, Viola, and Ferreira (2013); Tornabene, Viola, and Fantuzzi (2013)]. Thus, mapping technique must refer to every sub-domain in order to transform the physical coordinates x-y into the parent element coordinates ξ-η. The general mapping transformation, that is the same as in FEM, can be written as follows

$$x = x(\xi), \quad y = y(\eta) \tag{8}$$

Deriving the Cartesian mapping and applying the derivative laws, from Eq. 8 one gets

$$\frac{\partial}{\partial x} = \frac{\partial \xi}{\partial x}\frac{\partial}{\partial \xi} + \frac{\partial \eta}{\partial x}\frac{\partial}{\partial \eta}, \quad \frac{\partial}{\partial y} = \frac{\partial \xi}{\partial y}\frac{\partial}{\partial \xi} + \frac{\partial \eta}{\partial y}\frac{\partial}{\partial \eta} \tag{9}$$

Since a higher order computational scheme is solved in this work, the second order derivatives have to be calculated

$$\begin{aligned}
\frac{\partial^2}{\partial x^2} &= \frac{\partial^2 \xi}{\partial x^2}\frac{\partial}{\partial \xi} + \frac{\partial^2 \eta}{\partial x^2}\frac{\partial}{\partial \eta} + \left(\frac{\partial \xi}{\partial x}\right)^2 \frac{\partial^2}{\partial \xi^2} + \left(\frac{\partial \eta}{\partial x}\right)^2 \frac{\partial^2}{\partial \eta^2} + 2\frac{\partial \xi}{\partial x}\frac{\partial \eta}{\partial x}\frac{\partial^2}{\partial \xi \partial \eta} \\
\frac{\partial^2}{\partial y^2} &= \frac{\partial^2 \xi}{\partial y^2}\frac{\partial}{\partial \xi} + \frac{\partial^2 \eta}{\partial y^2}\frac{\partial}{\partial \eta} + \left(\frac{\partial \xi}{\partial y}\right)^2 \frac{\partial^2}{\partial \xi^2} + \left(\frac{\partial \eta}{\partial y}\right)^2 \frac{\partial^2}{\partial \eta^2} + 2\frac{\partial \xi}{\partial y}\frac{\partial \eta}{\partial y}\frac{\partial^2}{\partial \xi \partial \eta} \\
\frac{\partial^2}{\partial x \partial y} &= \frac{\partial^2 \xi}{\partial x \partial y}\frac{\partial}{\partial \xi} + \frac{\partial^2 \eta}{\partial x \partial y}\frac{\partial}{\partial \eta} + \frac{\partial \xi}{\partial x}\frac{\partial \xi}{\partial y}\frac{\partial^2}{\partial \xi^2} + \frac{\partial \eta}{\partial x}\frac{\partial \eta}{\partial y}\frac{\partial^2}{\partial \eta^2} + \\
&+ \left(\frac{\partial \xi}{\partial x}\frac{\partial \eta}{\partial y} + \frac{\partial \xi}{\partial y}\frac{\partial \eta}{\partial x}\right)\frac{\partial^2}{\partial \xi \partial \eta}
\end{aligned} \tag{10}$$

The first and second order Cartesian derivatives of Eqs. 9, 10 are used to map the fundamental equations and the boundary conditions of the two-dimensional plane problem at hand. The interested reader can find all the details about coordinate transformation and mapping technique applied to differential quadrature in the works by [Cen, Chen, Li, and Fu (2009); Liu (1999); Xing and Liu (2009); Zong and Zhang (2009)]. As it is well-known, the GDQ technique evaluates a partial, or total, derivative of a function at a point as a weighted sum of some coefficients $a_{ij}^{(n)}$ for the corresponding values of the function at issue. In considering a one-dimensional problem, the GDQ technique allows to write the first order derivative as

$$\left.\frac{df(x)}{dx}\right|_{x=x_i} \cong \sum_{j=1}^{N} a_{ij}^{x,(1)} f(x_j), \quad i=1,2,\ldots,N \tag{11}$$

where N is the total number of collocation points and $a_{ij}^{x,(1)}$ are the weighting coefficients, evaluated using Lagrange interpolation polynomials L. These test functions can be found in literature [Civan and Sliepcevich (1984); Bert and Malik (1997); Tornabene, Viola, and Inman (2009); Viola, Dilena, and Tornabene (2007); Tornabene, Marzani, Viola, and Elishakoff (2010); Tornabene, Fantuzzi, Viola, Cinefra, Carrera, Ferreira, and Zenkour (2014)] and have the form

$$L^{(1)}(x_i) = \prod_{q=1,q\neq i}^{N} (x_q - x_i), \quad L^{(1)}(x_j) = \prod_{q=1,q\neq j}^{N} (x_q - x_j) \tag{12}$$

The weighting coefficients of the second and higher order derivatives can be computed from recurrence relationships [Shu (2000); Viola, Rossetti, and Fantuzzi (2012); Ferreira, Viola, Tornabene, Fantuzzi, and Zenkour (2013); Tornabene, Fantuzzi, Viola, and Carrera (2014)]. A generalized higher order derivative can be written as

$$\begin{aligned} &\left.\frac{d^n f(x)}{dx^n}\right|_{x=x_i} = f_x^{(n)}(x_i) = \sum_{j=1}^{N} a_{ij}^{x,(n)} f(x_j) \\ &\text{for } i=1,2,\ldots,N,\ n=2,3,\ldots,N-1 \end{aligned} \tag{13}$$

This general approach based on the polynomial approximation, as shown in [Viola, Tornabene, and Fantuzzi (2013a,c); Tornabene, Fantuzzi, Viola, and Reddy (2014);

Tornabene and Reddy (2013)], allows to write the following weighting coefficients

$$\begin{aligned} a_{ij}^{x,(n)} &= n\left(a_{ii}^{x,(n-1)}a_{ij}^{x,(1)} - \frac{a_{ij}^{x,(n-1)}}{x_i - x_j}\right) \quad \text{for } i \neq j,\ n = 2,3,\ldots,N-1 \\ a_{ii}^{x,(n)} &= -\sum_{k=1,k\neq i}^{N} a_{ik}^{x,(n)} \qquad\qquad\qquad\qquad\qquad\qquad \text{for } i = j \end{aligned} \tag{14}$$

There are various articles about the GDQ weighting coefficients calculation, that it is impossible to cite them all. Among others, here are mentioned the ones by [Shu, Chen, and Du (2000); Tornabene, Liverani, and Caligiana (2011, 2012a,b,c); Tornabene and Viola (2007, 2008, 2009a,b, 2013)]. Since cracks lead to high stress concentrations at their tips, in the following numerical examples a localized version of GDQ has been worked out. In particular, Local Generalized Differential Quadrature (LGDQ) has been considered as introduced in literature by [Sun and Zhu (2000); Zong and Lam (2002); Lam, Zhang, and Zong (2004); Shen, Young, Lo, and Sun (2009); Tsai, Young, and Hsiang (2011); Hamidi, Hashemi, Talebbeydokhti, and Neill (2012); Tornabene (2012); Nassar, Matbuly, and Ragb (2013); Wang, Cao, and Ge (2013); Yilmaz, Girgin, and Evran (2013)]. The main difference between LGDQ and GDQ is that in the former the nth-order derivative of $f(x)$ is computed locally as

$$\left.\frac{d^n f(x)}{dx^n}\right|_{x=x_i} \cong \sum_{j=1}^{N_i} \bar{a}_{ij}^{x,(n)} f(x_j), \quad i = 1,2,\ldots,N_i \tag{15}$$

where N_i are the points of the local domain around the point x_i as depicted in Fig. 2. The overline of $a_{ij}^{(n)}$ in Eq. 15 denotes the different weighting coefficients from the ones corresponding to the GDQ method. In this way, the local numerical error at the crack tip does not propagate through the GDQ domain due to its local numerical scheme.

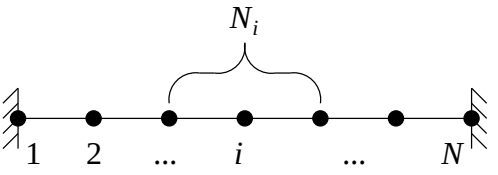

Figure 2: Local GDQ scheme.

4 Examples

In the study, the static and dynamic behaviour of two dimensional structures containing cracks and discontinuities is mainly investigated by the GDQFEM. It is recalled that the aim of this paper is not to study the fracture mechanics of 2D solids, but to show some numerical applications and comparisons of plane structures with discontinuities that do not consider the stress and strain singularities at the crack tip. The numerical analysis can be divided into two main parts. In the first part some benchmark tests are performed. A comparison with the FEM results is also performed. Moreover, some unpublished results about composite structures with discontinuities are presented. In the second part of this section, a cracked structure is examined by considering not only homogeneous materials but also composite materials. In particular two different numerical techniques are used in the following. In the first part the classic GDQ is applied. A Chebyshev-Gauss-Lobatto (C-G-L) grid distribution is used for all the computations. The C-G-L points are located as

$$\xi_i, \eta_i = -\cos\left(\frac{i-1}{N-1}\pi\right), \text{ for } i = 1,\ldots,N \tag{16}$$

where ξ and η are the parent element coordinates involved in the mapping transformation and $\xi, \eta \in [-1,1]$. When cracked structures are investigated the local GDQ method is used, since it reduces the error propagation. Hence, a uniform grid distribution is employed

$$\xi_i, \eta_i = \frac{i-1}{N-1}, \text{ for } i = 1,\ldots,N \tag{17}$$

4.1 Cantilever wall

The accuracy of the GDQFEM technique is explored by examining the in-plane vibration of the square cantilever plate shown in Fig. 3. It can be viewed as a kind of beam under the plane stress condition. This cantilever wall is a consolidated FEM benchmark through literature [Gupta (1978); Cook and Avrashi (1992); Zhao and Steven (1996); de Miranda, Molari, and Ubertini (2008)]. In fact, this problem has been studied in great detail and a reference solution was obtained by using a very fine FEM mesh of the plane stress under consideration. In addition to the other assessments that can be found in the aforementioned papers, here a different and alternative solution for the same problem is worked out using GDQFEM. The present solution is searched through the strong formulation of the elasticity problem at issue. The previous papers [Gupta (1978); Cook and Avrashi (1992); Zhao and Steven (1996); de Miranda, Molari, and Ubertini (2008)] used FEM and adopted a

Table 1: First ten eigenfrequencies of a cantilever wall.

ω	Ref. †	FEM	GDQFEM $n_e = 1$			
[rad/s]			$N = 11$	$N = 21$	$N = 31$	$N = 41$
1	0.065853	0.065820	0.065917	0.065828	0.065819	0.065816
2	0.157951	0.157956	0.157948	0.157948	0.157950	0.157951
3	0.176908	0.177207	0.177197	0.177206	0.177206	0.177205
4	0.279651	0.281591	0.281572	0.281588	0.281590	0.281590
5	0.30337	0.303671	0.303475	0.303636	0.303652	0.303656
6	0.321367	0.322280	0.322276	0.322281	0.322280	0.322280
7	-	0.406225	0.406195	0.406225	0.406223	0.406223
8	-	0.427679	0.427694	0.427663	0.427662	0.427662
9	-	0.472234	0.472220	0.472235	0.472233	0.472233
10	-	0.475256	0.475288	0.475252	0.475249	0.475248
ω	GDQFEM $n_e = 4$ (Regular)			GDQFEM $n_e = 4$ (Distorted)		
[rad/s]	$N = 7$	$N = 11$	$N = 21$	$N = 7$	$N = 11$	$N = 21$
1	0.065952	0.065845	0.065818	0.065794	0.065826	0.065819
2	0.157974	0.157952	0.157951	0.158004	0.157952	0.157950
3	0.177241	0.177218	0.177208	0.177212	0.177217	0.177210
4	0.281638	0.281595	0.281591	0.281752	0.281601	0.281592
5	0.303666	0.303665	0.303661	0.303519	0.303671	0.303667
6	0.322306	0.322286	0.322281	0.322317	0.322287	0.322282
7	0.406221	0.406209	0.406222	0.406472	0.406213	0.406226
8	0.427720	0.427660	0.427665	0.427872	0.427694	0.427678
9	0.472557	0.472227	0.472232	0.472759	0.472242	0.472233
10	0.475375	0.475225	0.475243	0.475507	0.475209	0.475239

† [Zhao and Steven (1996)]

weak formulation of the differential system of equations. In Fig. 3a) the problem geometry is graphically depicted, where the width of the given cantilever wall is $L = 10$ m. The material is elastic, homogeneous and isotropic and its Young's modulus is $E = 1$ Pa, Poisson's ratio $\nu = 0.3$ and density $\rho = 1$ kg/m^3.

Three different meshes are taken into account: a single element mesh $n_e = 1$, a four element mesh $n_e = 4$ (see Fig. 3b)) and a four element distorted mesh $n_e = 4$ (see Fig. 3c)). It is noted that one of the four distorted elements of Fig. 3c) shows a high distortion degree. The GDQFEM element used in this computation is an 8 node element. The numerical results in terms of circular frequencies are summarized in Tab. 1 where the FEM reference solution and the GDQFEM solution obtained with

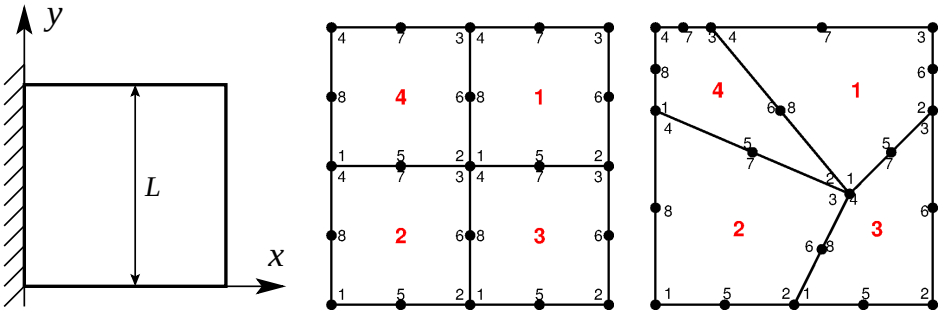

(a) (b) (c)

Figure 3: Cantilever wall: a) Model geometry; b) GDQFEM four element regular mesh; c) GDQFEM four element highly distorted mesh.

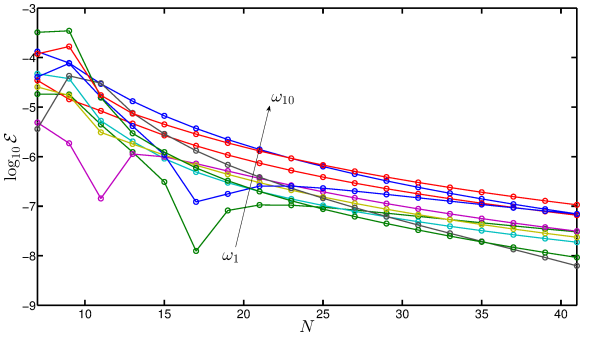

(a)

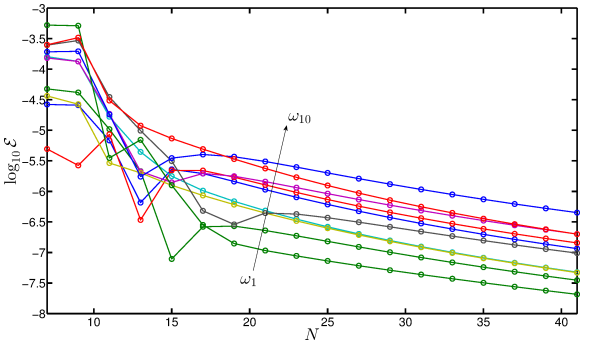

(b)

Figure 4: Convergence tests for a cantilever wall: a) Four regular elements; b) Four elements within a highly distorted mesh.

several meshes are shown. Very good agreement is observed among all the computations. For each numerical case the same number of points along the master element coordinates is considered $N = M$. A detailed accuracy test is presented in Fig. 4, where the logarithm of the absolute error $\mathscr{E} = |\omega_{\text{GDQFEM}} - \omega_{\text{FEM}}|$, between GDQFEM and FEM numerical solutions, is reported as a function of the number of grid points per element. In particular, in Fig. 4a) the four element regular mesh is examined, whereas in Fig. 4b) the four element distorted mesh is investigated. It is noted that the error increases if a distorted mesh is used. However, for each frequency the graphs always tend to decrease when the number of points per element N is increased. The convergence tests of Fig. 4 involve the first ten circular frequencies. For both meshes a good agreement is achieved for the higher frequency modes, which are usually the controlling factors for the accuracy assessment of a finite element solution.

4.2 Tapered cantilever plate with a central circular hole

In the second benchmark the vibration of a tapered cantilever plate with a central circular hole under plane stress conditions is considered. The aim of this application is to examine the accuracy and applicability of the present methodology when irregular and unstructured meshes are used. In fact, it should be noted that in the previous case multi-domain GDQ could be applied when regular squared elements were used. On the contrary, distorted elements with curved boundaries are used in the following. The plate geometry is represented in Fig. 5a) where the greatest side is $L = 10$ m and the inner hole radius is $R = 1.5$ m. In particular the hole centre has coordinates $(5,5)$ m and the shortest side is $l = 5$ m. The tapered plate shows one symmetry axis. This geometry has been also studied by several authors [Zhao and Steven (1996); de Miranda, Molari, and Ubertini (2008)]. Regarding the material, it is assumed, isotropic and homogeneous with elastic modulus $E = 1$ Pa, Poisson's ratio $\nu = 0.3$ and density $\rho = 1$ kg/m^3. The reference FEM solution is evaluated using the mesh illustrated in Fig. 5b) where $n_e = 7312$ using S8R element type. Two different GDQFEM meshes were used in the computations: a four element mesh $n_e = 4$ (see Fig. 5c)) and an eight element mesh $n_e = 8$ (see Fig. 5d)). This choice has been made in order to map differently the circular internal hole. It has been shown from Figs. 5c)-d) that four elements are the minimum number of elements for a good mapping of circular shapes. The first ten circular frequencies of Tab. 2 show that the eight node mesh leads to a more accurate convergence than the four element mesh. To summarize, the absolute circular frequency error, of the first ten frequencies, is plotted as a function of the number of grid points per element for the two meshes at issue. The accuracy tests represented in Fig. 6a) show the results obtained with a four element mesh. In Fig. 6b) an eight element mesh has been

used. It appears that the solution obtained with $n_e = 8$ is 10 times more accurate than the solution with $n_e = 4$ for the same amount of grid points per element.

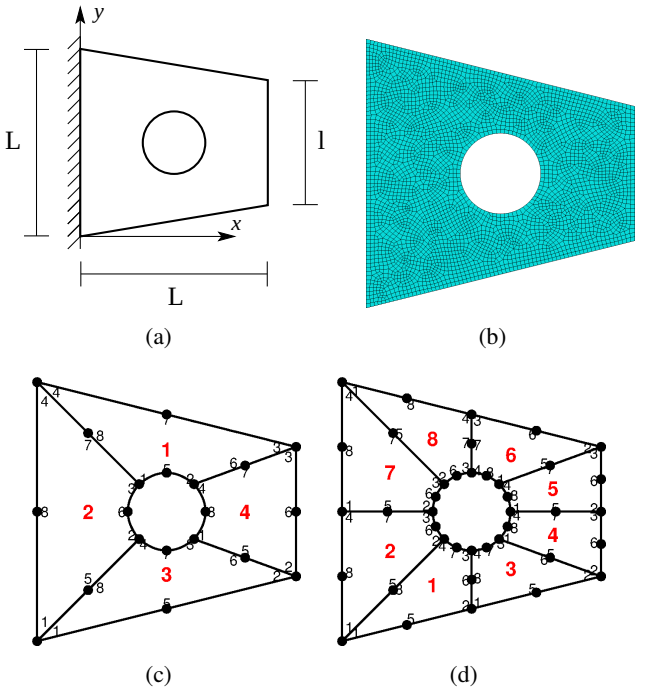

Figure 5: Cantilever tapered plate with a central circular hole: a) Model geometry; b) FEM mesh with $n_e = 3712$ using 8 node S8R Abaqus elements; c) Four element mesh; d) Eight element mesh.

4.3 Square plate with circular hole

In the next numerical application, the classic problem of a homogeneous plate with a circular centred hole is considered under static loading. In Fig. 7a) the problem geometry is depicted, where the dimensional plate parameter is $L = 5$ m and the applied normal tension is $\sigma = 100$ N/m. The material has a Young's modulus $E = 3 \cdot 10^7$ Pa and Poisson's ratio $\nu = 0.3$. The numerical solutions are presented in terms of the normal stress σ_y calculated at any point of the line segment AB, from the point A at the circular edge to the external point B of the plate straight edge. Every stress distribution is computed for a fixed value of the geometrical ratio $\chi = D/L$ between the diameter D of the hole and the plate side length L. The side L remains constant in all the calculations. The GDQFEM mesh used in the

Table 2: First ten eigenfrequencies of a tapered cantilever plate with a circular central hole.

ω [rad/s]	FEM	GDQFEM $n_e = 4$			GDQFEM $n_e = 8$		
		$N = 11$	$N = 21$	$N = 41$	$N = 11$	$N = 21$	$N = 31$
1	0.0700	0.071226	0.070128	0.070120	0.069976	0.069978	0.069978
2	0.1558	0.155596	0.155998	0.155998	0.155851	0.155863	0.155864
3	0.1999	0.199411	0.199967	0.199962	0.199874	0.199880	0.199879
4	0.2620	0.262110	0.262643	0.262636	0.262028	0.262070	0.262071
5	0.2917	0.292303	0.292199	0.292197	0.291744	0.291732	0.291732
6	0.4192	0.419199	0.419846	0.419847	0.419260	0.419256	0.419259
7	0.4208	0.420896	0.420925	0.420918	0.420825	0.420818	0.420818
8	0.4678	0.468142	0.468025	0.468024	0.467834	0.467844	0.467845
9	0.4801	0.480427	0.480894	0.480894	0.480190	0.480122	0.480124
10	0.5281	0.525467	0.528197	0.528203	0.528079	0.528074	0.528076

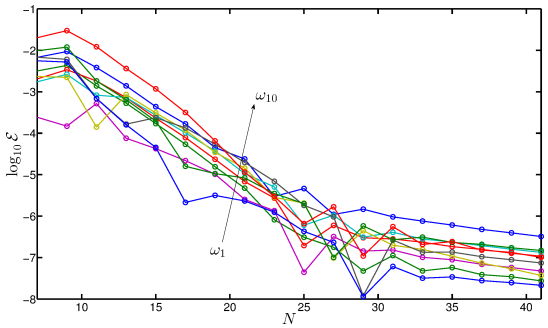

(a)

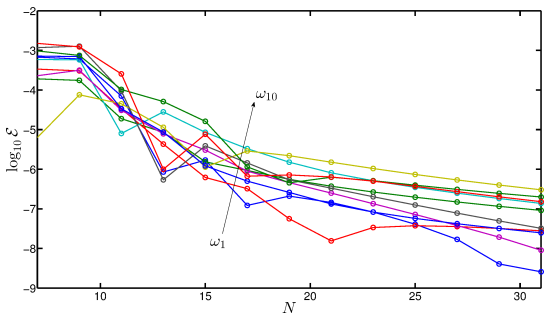

(b)

Figure 6: Convergence tests for a tapered cantilever plate with a central circular hole: a) Four element mesh; b) Eight element mesh.

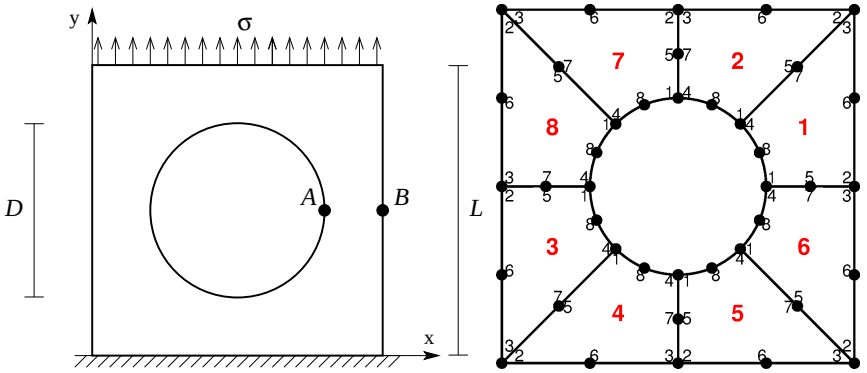

(a) (b)

Figure 7: Square plate with a centred circular hole subjected to tension σ: a) Geometric representation; b) GDQFEM mesh.

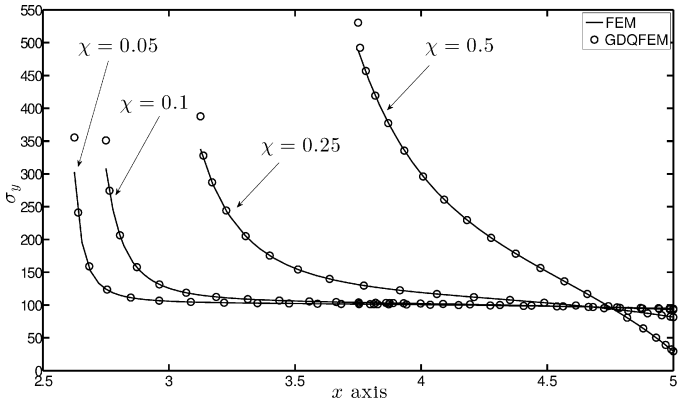

Figure 8: Stress profiles of a square plate subjected to tension $\sigma = 100$ N/m with a central circular hole .

computations, for $\chi = 0.5$ and $\chi = 0.25$, is an eight element mesh with 8 node per element as shown in Fig. 7b). For every calculation a $N = 21$ C-G-L grid points is used. For the other two cases ($\chi = 0.1$ and $\chi = 0.05$) sixteen elements and $N = 15$ are used. As it can be noted from Fig. 8 the GDQFEM solution is superimposed to the FEM solution for every χ value. Furthermore, when the plate side is four times greater than the circle diameter the normal stress σ_y tends to the applied stress value $\sigma = 100$ N/m and the tip stress value tends to be three times the applied load, as it is very well-known from the literature, when the dimension $L \to \infty$. It should be underlined that the abscissa of Fig. 8 is the horizontal line between point A and B

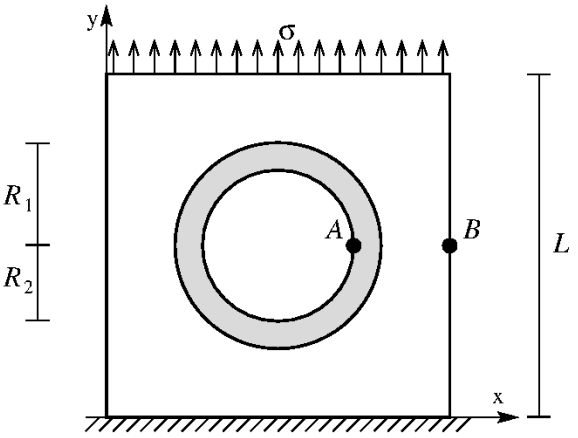

Figure 9: Square plate subjected to tensile stress σ with a centred hollow inclusion.

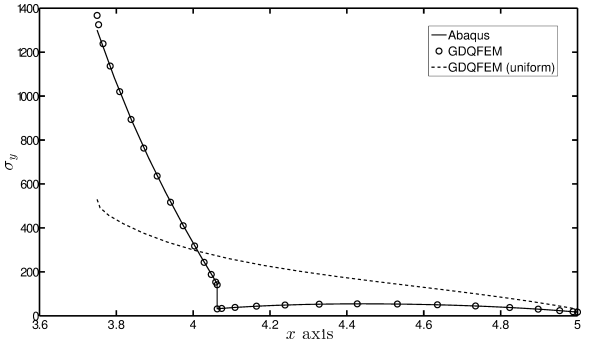

Figure 10: Stress profile of a square plate subjected to tensile stress $\sigma = 100$ N/m with a centred elastic hollow inclusion.

of Fig. 7a), where the point B is fixed at $x = 5$ m and point A moves from $x = 2.625$ m to $x = 3.75$ m (because the circular hole diameter decreases, whereas the plate remains of the same size).

In order to study the interaction effect between a matrix containing a circular hole and a hollow elastic inclusion, the system depicted in Fig. 9 is investigated. The plate side is $L = 5$ m, the outer radius is $R_1 = 1.5625$ m and the inner radius $R_2 = 1.25$ m. The external normal load is $\sigma = 100$ N/m. The soft matrix has $E_m = 3 \cdot 10^6$ Pa and Poisson's ratio $\nu_m = 0.25$, whereas the inner hollow inclusion is made of a harder material with $E_i = 3 \cdot 10^7$ Pa and $\nu_i = 0.3$. In Fig. 10 the stress profile involving the points between A and B is graphically shown. The single dashed curve represents the homogeneous case, presented above and where only the matrix

material is present. The presence of a hollow inclusion gives rise to an abrupt jump at the material interface between the two materials. The GDQFEM solution with black circles is superimposed to the solid FEM line.

4.4 Soft-core elliptic arch

In the last benchmark the free vibrations of a composite three layer soft-core elliptic arch with elliptic holes is presented. The two external layers are made of a material which is stiffer than the one that the core layer is made of. Fig. 11 shows the GDQFEM mesh used in the computation. The soft-core arch is clamped on the horizontal axis and free along its curvilinear edges, as well as along the boundary of the holes. The darker elements refer to the two stiffer sheets with $E_s = 3 \cdot 10^9$ Pa, $\nu_s = 0.3$ and $\rho_s = 1000$ kg/m^3. The inner soft-core has $E_c = 3 \cdot 10^7$ Pa, $\nu_c = 0.25$ and $\rho_c = 500$ kg/m^3, instead. The dimensions of the outer ellipse are $a_1 = 10$ m, $b_1 = 5$ m, whereas the inner ellipse is defined by $a_2 = 5$ m, $b_2 = 2.5$ m, where a_1, b_1 and a_2, b_2 are the semi-diameters of the ellipses in hand. The structure has a vertical symmetry and variable radii of curvature. The location and the dimensions of the three elliptic holes can be deducted according to the drawing scale of the elliptic soft-core embedded between the external layers of the arch shown in Fig. 11. The major axis of symmetry of each elliptic hole is tangent to the elliptic soft-core axis at the point specified by the center of the elliptic hole itself. The GDQFEM uses 44 elements of irregular shape with various grid point number as reported in Tab. 3, where the GDQFEM convergence is also shown. Very good agreement is observed between the FEM solution and the GDQFEM numerical results obtained with the mesh of Fig. 11. It appears that few grid points are sufficient to obtain an accurate solution, since here a high number of elements has been used. For the sake of completeness, the first four modal shapes of the structure at issue are shown in Fig. 12, where the soft-core behaviour of the structure is clearly displayed by the deformed mode shapes.

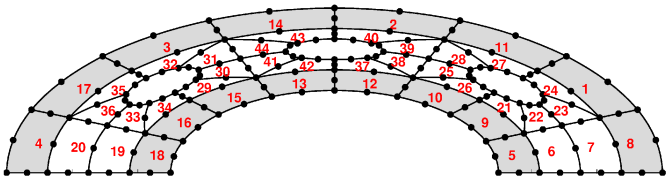

Figure 11: Geometric representation of an elliptic soft-core arch with holes.

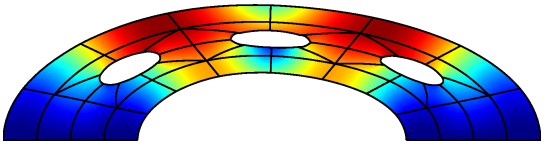

1st mode

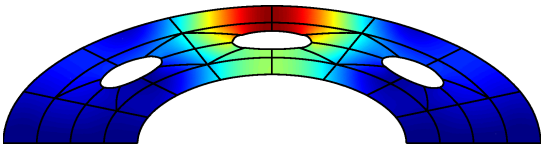

2nd mode

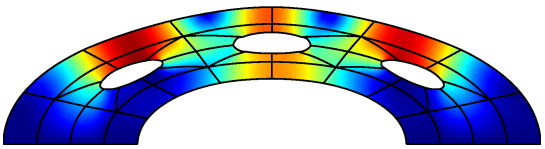

3rd mode

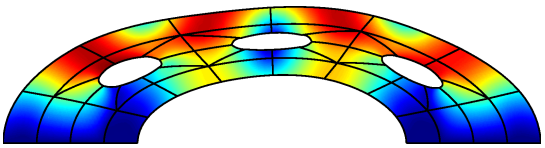

4th mode

Figure 12: First four modal shapes for an elliptic soft-core arch with holes.

Table 3: First ten frequencies of the hollow soft-core elliptic arch.

f [Hz]	FEM	GDQFEM		
		$N=9$	$N=11$	$N=13$
1	25.2318	25.2320	25.2691	25.2757
2	31.0079	31.8934	31.5975	31.4676
3	45.6878	45.9543	45.8373	45.8205
4	46.5109	47.9696	47.4468	47.1375
5	56.1484	57.5597	57.1569	56.8099
6	65.019	65.3243	65.2754	65.2259
7	70.9465	71.0756	70.9368	70.9230
8	74.8534	75.7430	75.4100	75.1430
9	87.995	88.2576	88.2303	88.2124
10	91.3028	91.5527	91.6743	91.6779

4.5 Bi-material edge crack problem

In the following a bi-material edge crack problem is studied. The structure under consideration is a rectangular plate with an edge linear through-the-thickness crack where $L = 16$ m, $D = 7$ m and $a = 3.5$ m as depicted in Fig. 13. Different configurations are shown in dealing with homogeneous and bi-material cases under tensile stress and shear force. The two homogeneous and isotropic materials used in the following computations are characterized by the corresponding mechanical parameters: $E_1 = 1000$ Pa, $\nu_1 = 0.3$ for material 1 and $E_2 = 100$ Pa, $\nu_2 = 0.3$ for material 2. Both tangential and normal loads have the same intensity: $q = 3.42857$ N/m. For each loading condition, the normal stress σ_y has been computed using FEM, CM and GDQFEM for the three distinct sections indicated in Figs. 13a)-b) ($\theta = 0, +45, -45$). The meshes used for computations according to CM, FEM and GDQFEM are shown in Fig. 14. It is noted that the CM mesh is composed of $n_e = 2668$. The FEM mesh has $n_e = 6125$, where a strong refinement is present around the crack tip with collapsed eight node elements [Pu, Hussain, and Lorensen (1978); Anderson (1995)]. Finally, the GDQFEM mesh is made of four elements ($n_e = 4$), where 21×21 grid points per elements are used. In the following several representations are shown for different cases. For the edge cracked plate under shear loading, the σ_y numerical results are reported in Figs. 15-20. In the second group of figures depicted in Figs. 21-26, the same plate model is studied under uniform tension. For each group four different cases are studied: two homogeneous cases (when material 1 and material 2 are the same) and two bi-material systems, where the material 1 is set below the crack and material 2 above and vice versa. The static analysis results are presented in terms of σ_y stress comparison. Plots involving points of the contour, and cross sections of the system for the crack tip, are shown and discussed. Starting from the uniform shear stress applied at the top of the cracked plate (see Figure 13a)), the stress contour plot comparison for the two homogeneous cases are depicted in Fig. 15 for the material 1 case and in Fig. 16 for the material 2 case. It is observed that the color maps obtained though the CM, FEM and GDQFEM are similar among them. On the other hand, looking at the composite system graphically reported in Fig. 17, when material 1 is below the line crack and material 2 is above the crack itself, and in Fig. 18, when material 2 is below the line crack and material 1 is above the crack, very good agreement is observed between all the computations.

As far as the normal stress σ_y comparison is concerned, the plots in Figs. 19-20 show the solid blue line to indicate the CM solution, the line made of black crosses is the FEM solution and, finally, the line made of black circles represents the GDQFEM solution. In detail, Figs. 19a)-c) show the homogeneous material 1 case, where σ_y is represented at $\theta = 0^\circ$, $\theta = +45^\circ$ and $\theta = -45^\circ$. Figs. 19d)-f)

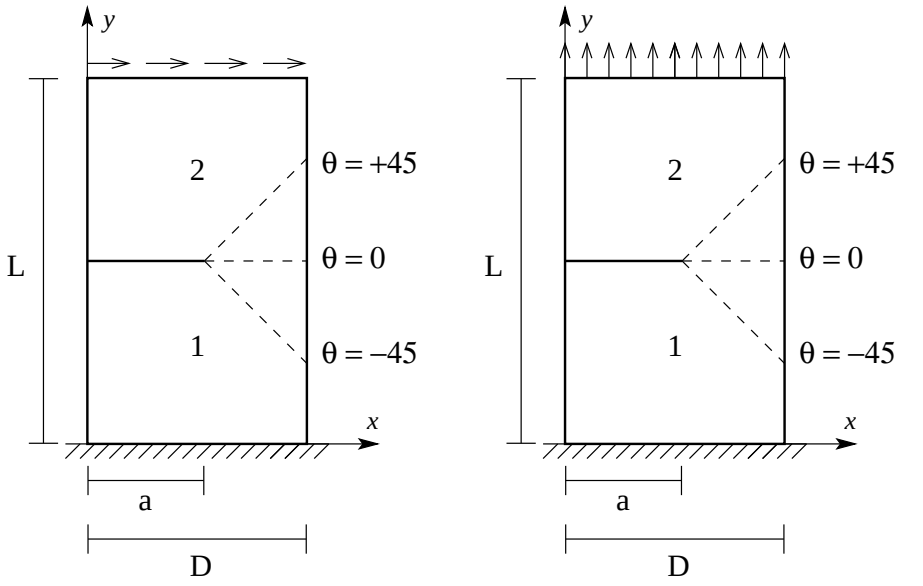

Figure 13: Edge crack plate configurations: a) when a shear force is applied; b) when a normal stress is applied.

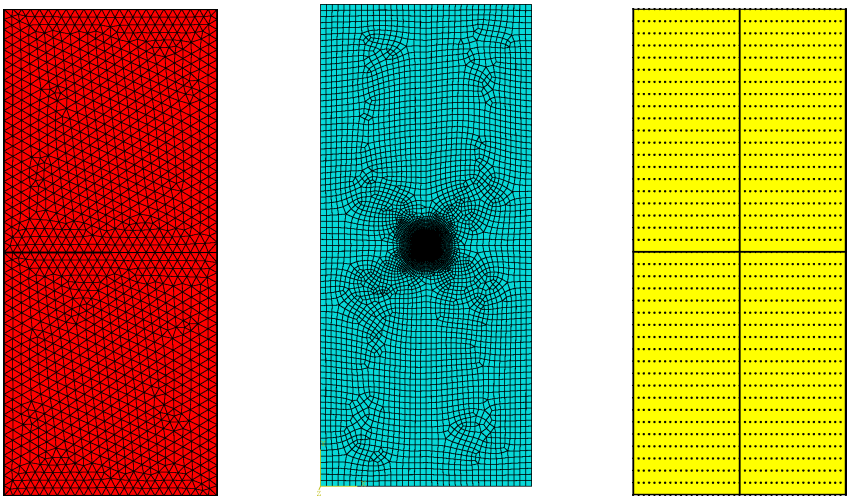

Figure 14: Used meshes: a) CM; b) FEM; c) GDQFEM.

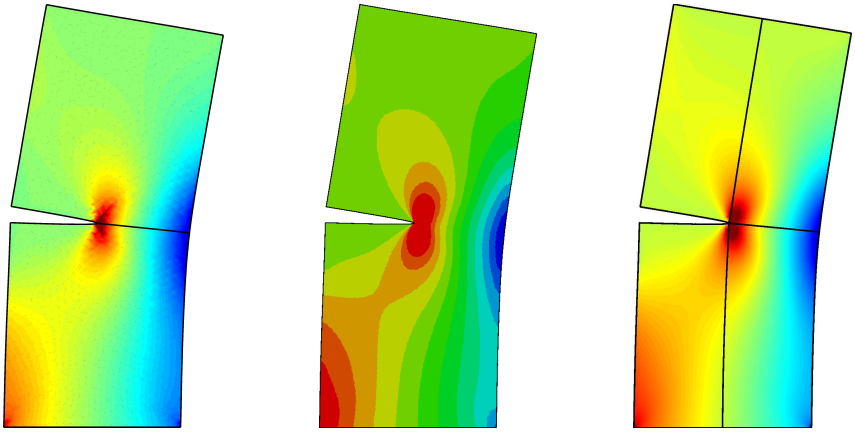

(a) (b) (c)

Figure 15: Normal stress σ_y comparison for the homogeneous material 1 under shear: a) CM; b) FEM; c) GDQFEM.

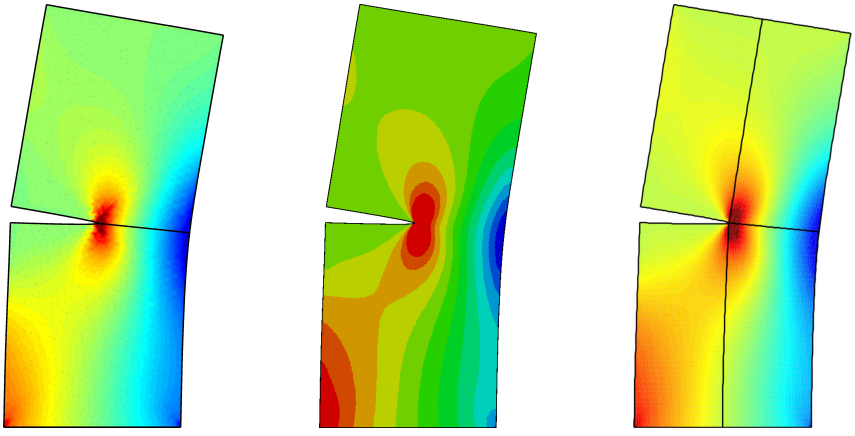

(a) (b) (c)

Figure 16: Normal stress σ_y comparison for the homogeneous material 2 under shear: a) CM; b) FEM; c) GDQFEM.

present the homogeneous material 2 solution under shear for the same three sections ($\theta = 0°, +45°, -45°$). Comparisons for the bi-material system are reported in Figs. 20a)-f). Very good agreement is observed for all the investigated sections and all the numerical techniques. As second numerical application the uniform tensile stress $\sigma = 100$ N/m is considered. As in the previous example, the numerical results obtained by GDQFEM are compared with FEM and CM results at different

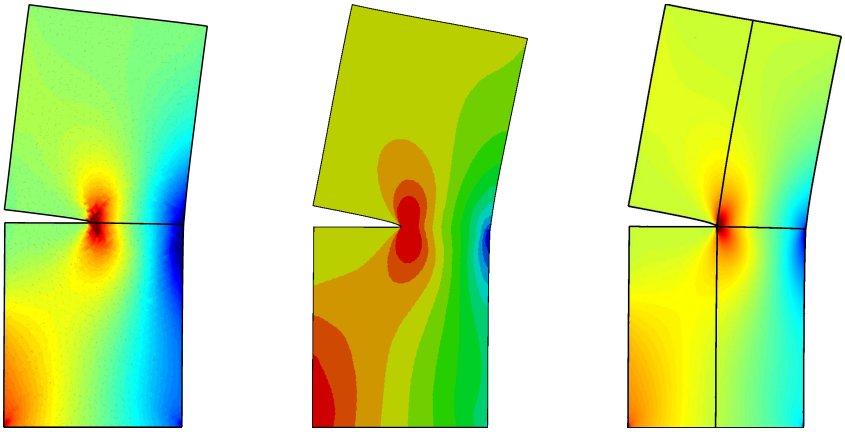

(a) (b) (c)

Figure 17: Normal stress σ_y comparison for the bi-material system as shown in Fig. 13 a): a) CM; b) FEM; c) GDQFEM.

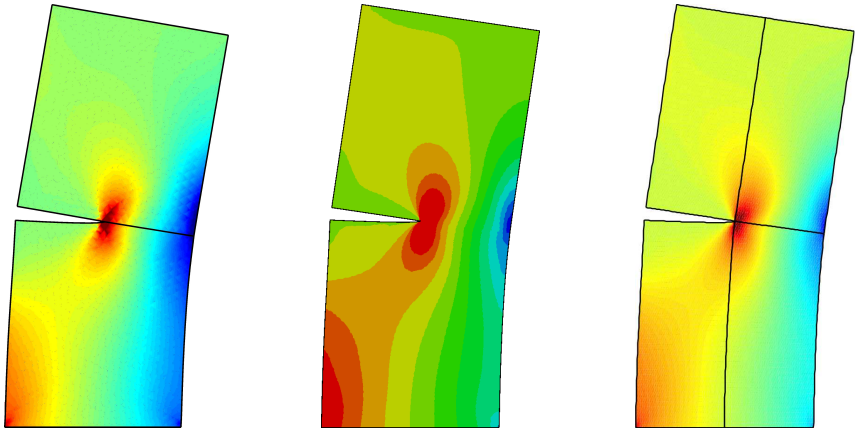

(a) (b) (c)

Figure 18: Normal stress σ_y comparison for the bi-material system: material 2 below and material 1 above under shear: a) CM; b) FEM; c) GDQFEM.

sections ($\theta = 0°$, $\theta = +45°$, $\theta = -45°$). Four material configurations are studied: two homogeneous cases and two bi-material cases. In Figs. 21-24 the normal stress σ_y contour plots are depicted for the three numerical techniques at issue. It is noted from the deformed shapes of Figs. 21-22 that the material is homogeneous above and below the line crack, whereas in Figs. 23-24 it is clear that the materials above and below the line crack are different, because one part deforms more than

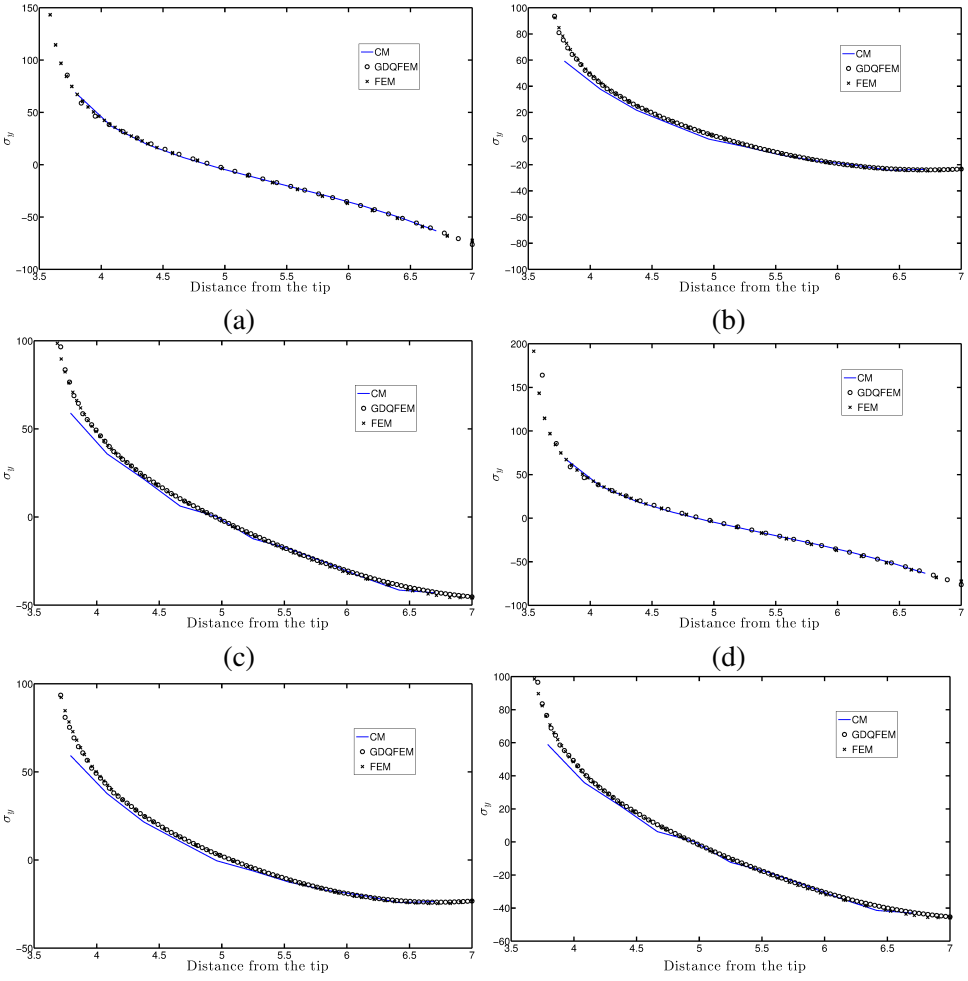

Figure 19: Normal stress profile σ_y for homogeneous material under shear: a) material 1 at $\theta = 0°$; b) material 1 at $\theta = +45°$; c) material 1 at $\theta = -45°$, d) material 2 at $\theta = 0°$; e) material 2 at $\theta = +45°$; f) material 2 at $\theta = -45°$.

the other one. Finally, Figs. 25-26 show the stress plots for the four aforementioned configurations. In all the reported plots the solid blue line represents the CM solution, the black crosses indicate the FEM solution and the black circles stand for the GDQFEM solution. For each cross section, all the graphs of Figs. 25-26 start at the crack tip and finish at the free edge of the given plate. Good agreement is observed among the CM, FEM and GDQFEM solutions.

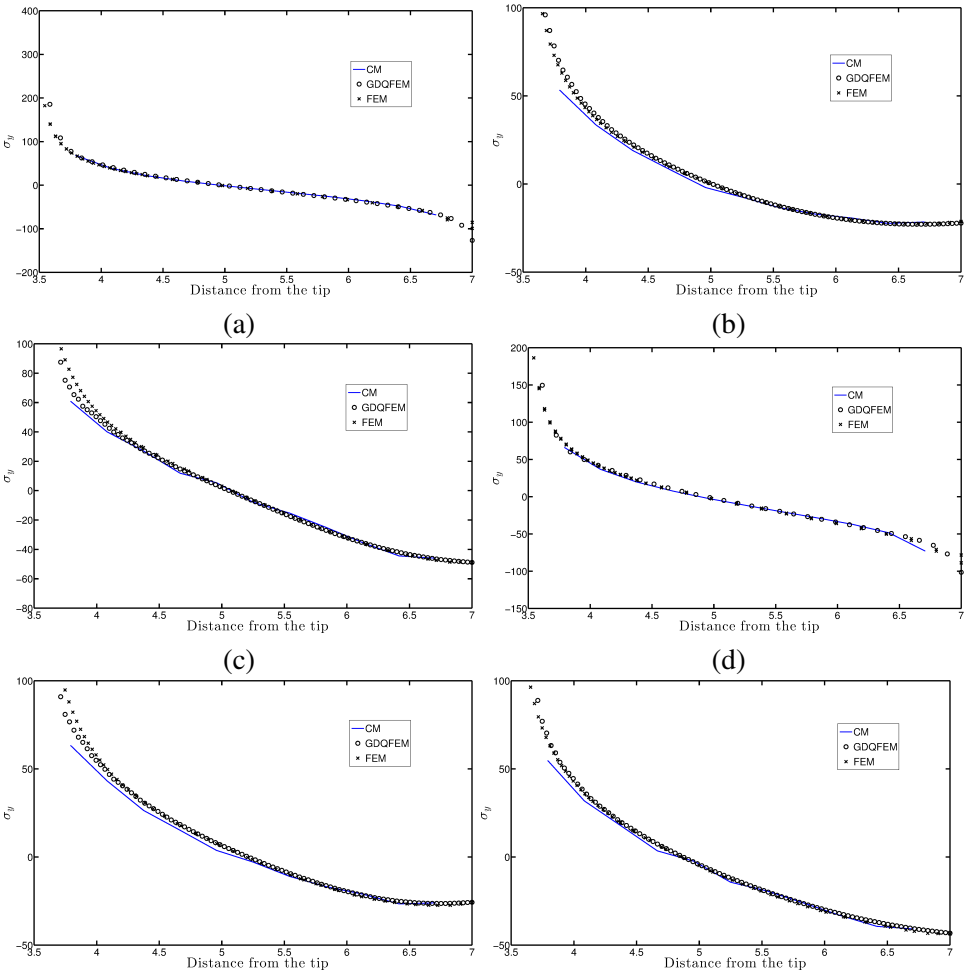

Figure 20: Normal stress profile σ_y for a bi-material system under shear: a) material 1 below and material 2 above at $\theta = 0°$; b) material 1 below and material 2 above at $\theta = +45°$; c) material 1 below and material 2 above at $\theta = -45°$, d) material 2 below and material 1 above at $\theta = 0°$; e) material 2 below and material 1 above at $\theta = +45°$; f) material 2 below and material 1 above at $\theta = -45°$.

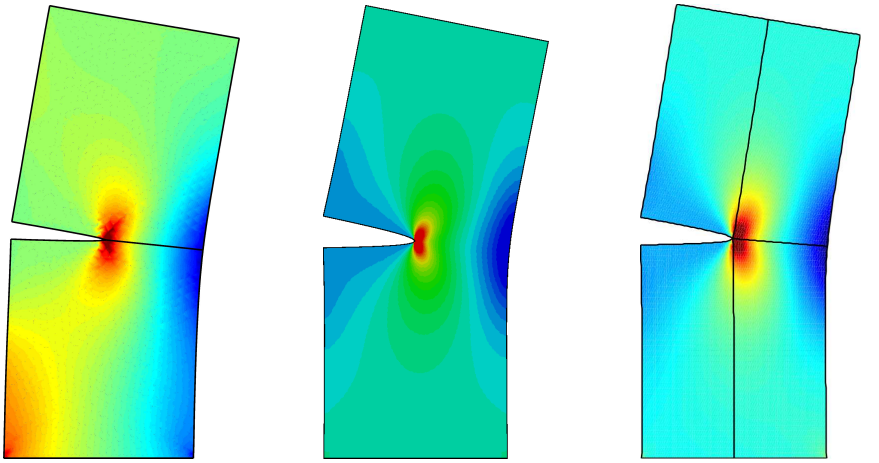

(a) (b) (c)

Figure 21: Normal stress σ_y comparison for the homogeneous material 1 under tensile stress: a) CM; b) FEM; c) GDQFEM.

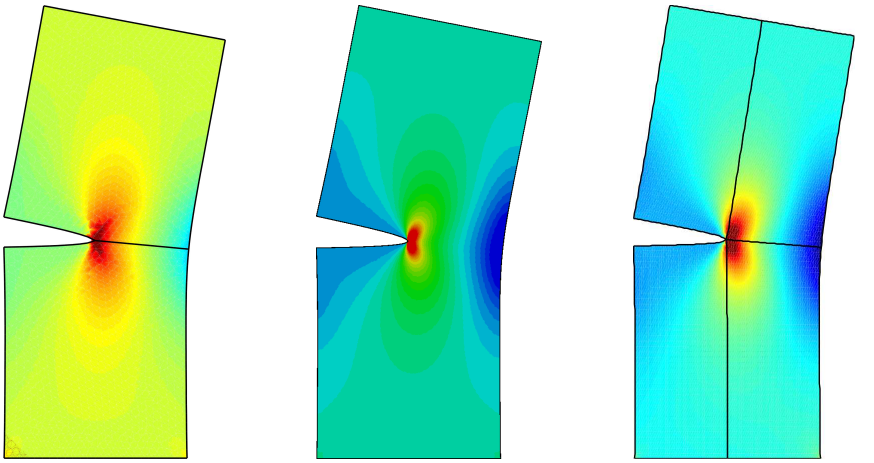

(a) (b) (c)

Figure 22: Normal stress σ_y comparison for the homogeneous material 2 under tensile stress: a) CM; b) FEM; c) GDQFEM.

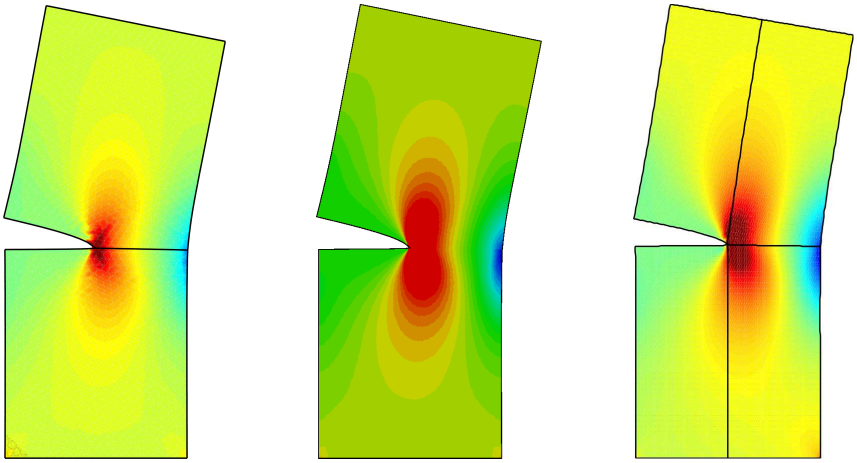

(a) (b) (c)

Figure 23: Normal stress σ_y comparison for the bi-material system as shown in Fig. 13b): a) CM; b) FEM; c) GDQFEM.

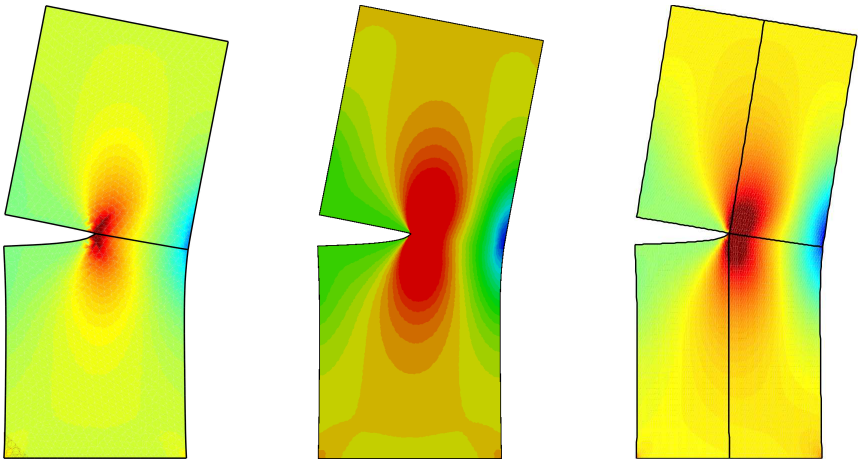

(a) (b) (c)

Figure 24: Normal stress σ_y comparison for the bi-material system: material 2 below and material 1 above under tensile stress: a) CM; b) FEM; c) GDQFEM.

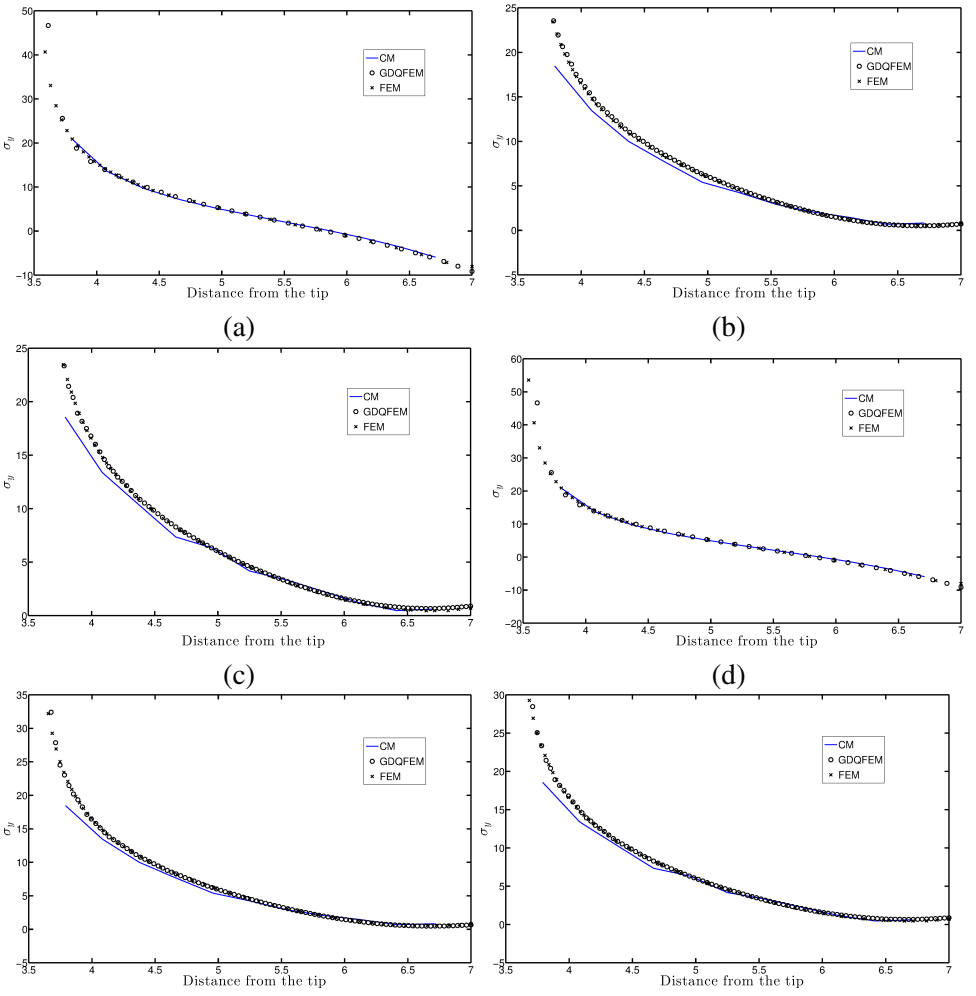

Figure 25: Normal stress profile σ_y for homogeneous material under tensile stress: a) material 1 at $\theta = 0°$; b) material 1 at $\theta = +45°$; c) material 1 at $\theta = -45°$, d) material 2 at $\theta = 0°$; e) material 2 at $\theta = +45°$; f) material 2 at $\theta = -45°$.

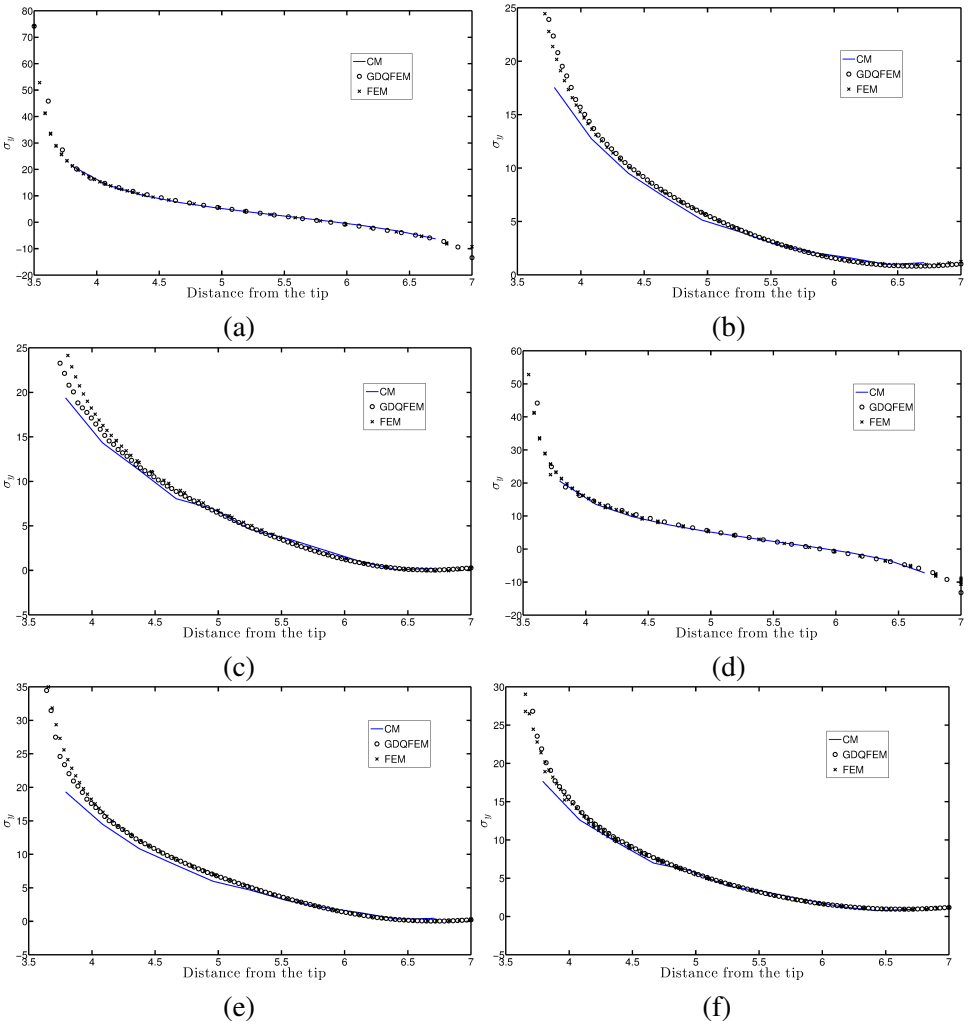

Figure 26: Normal stress profile σ_y for a bi-material system under tensile stress: a) material 1 below and material 2 above at $\theta = 0°$; b) material 1 below and material 2 above at $\theta = +45°$; c) material 1 below and material 2 above at $\theta = -45°$, d) material 2 below and material 1 above at $\theta = 0°$; e) material 2 below and material 1 above at $\theta = +45°$; f) material 2 below and material 1 above at $\theta = -45°$.

5 Conclusions

The main aim of this paper is to present several GDQFEM solutions to plane elastic problems with cracks and holes. The GDQFEM methodology differs from the FEM approach, since the former numerical procedure is based on the strong form of the differential system of equations, whereas the latter one starts from a weak formulation. As a result, the numerical solution gives the physical displacements of the model under consideration directly when the system is numerically solved.

It can be noted throughout the paper that GDQFEM leads to accurate and reliable results, in terms of both frequencies and stresses when compared with FEM and CM. Furthermore, the mesh-free GDQ character remains at the sub-domain level. Therefore, cracks and holes are treated through element decomposition, namely by dividing the physical domain into smaller parts. Since the approximation order can be imposed by the user, selecting more grid points N for each element, the GDQFEM elements have better convergence properties than the standard low order FEM elements implemented in commercial FEM codes. Finally, the GDQFEM numerical applicability is also general, because it can treat the model discontinuities increasing the number of elements in the global mesh n_e, having $\mathscr{C}^1$ continuity among them.

In the near future the cracked plate problem could be developed by considering an inclined crack and a biaxial loading condition [Carloni, Piva, and Viola (2003); Nobile, Piva, and Viola (2004)]. In addition, a comparison between the results associated to the plane stress condition at issue and the ones related to the formulation of a cracked beam element will be made [Viola, Nobile, and Federici (2002)].

Acknowledgement: This research was supported by the Italian Ministry for University and Scientific, Technological Research MIUR (40 % and 60 %). The research topic is one of the subjects of the Centre of Study and Research for the Identification of Materials and Structures (CIMEST)-"M. Capurso" of the University of Bologna (Italy).

References

Anderson, T. (1995): *Fracture Mechanics: Fundamentals and Applications, Second Edition*. CRC Press.

Artioli, E.; Gould, P. L.; Viola, E. (2005): A differential quadrature method solution for shear-deformable shells of revolution. *Engineering Structures*, vol. 27, no. 13, pp. 1879–1892.

Bert, C.; Malik, M. (1996): The differential quadrature method for irregular domains and application to plate vibration. *International Journal of Mechanical Sciences*, vol. 38, no. 6, pp. 589–606.

Bert, C. W.; Malik, M. (1997): Differential quadrature: a powerful new technique for analysis of composite structures. *Composite Structures*, vol. 39, no. 3-4, pp. 179–189.

Carloni, C.; Piva, A.; Viola, E. (2003): An alternative complex variable formulation for an inclined crack in an orthotropic medium. *Engineering Fracture Mechanics*, vol. 70, no. 15, pp. 2033–2058.

Cen, S.; Chen, X.-M.; Li, C. F.; Fu, X.-R. (2009): Quadrilateral membrane elements with analytical element stiffness matrices formulated by the new quadrilateral area coordinate method (QACM-II). *International Journal for Numerical Methods in Engineering*, vol. 77, no. 8, pp. 1172–1200.

Chen, C.-N. (1999): The development of irregular elements for differential quadrature element method steady-state heat conduction analysis. *Computer Methods in Applied Mechanics and Engineering*, vol. 170, no. 1-2, pp. 1–14.

Chen, C.-N. (1999): The differential quadrature element method irregular element torsion analysis model. *Applied Mathematical Modelling*, vol. 23, no. 4, pp. 309–328.

Chen, C.-N. (2003): DQEM and DQFDM for the analysis of composite two-dimensional elasticity problems. *Composite Structures*, vol. 59, no. 1, pp. 3–13.

Civan, F.; Sliepcevich, C. (1984): Differential quadrature for multi-dimensional problems. *Journal of Mathematical Analysis and Applications*, vol. 101, no. 2, pp. 423–443.

Civan, F.; Sliepcevich, C. M. (1985): Application of differential quadrature to solution of pool boiling in cavities. *Proceedings of the Oklahoma Academy of Science*, vol. 65, pp. 73–78.

Cook, R.; Avrashi, J. (1992): Error estimation and adaptive meshing for vibration problems. *Computers & Structures*, vol. 44, no. 3, pp. 619–626.

de Miranda, S.; Molari, L.; Ubertini, F. (2008): A consistent approach for mixed stress finite element formulations in linear elastodynamics. *Computer Methods in Applied Mechanics and Engineering*, vol. 197, no. 13-16, pp. 1376–1388.

Dong, L.; Atluri, S. (2012): Development of 3D T-Trefftz Voronoi cell finite elements with/without spherical voids &/or elastic/rigid inclusions for micromechanical modeling of heterogeneous materials. *CMC: Computers, Materials, & Continua*, vol. 29, no. 2, pp. 169–211.

Dong, L.; Atluri, S. (2013): Fracture & fatigue analyses: SGBEM-FEM or XFEM? Part 2: 3D solids. *CMES - Computer Modeling in Engineering and Sciences*, vol. 90, no. 5, pp. 379–413.

Dong, L.; Atluri, S. (2013): Fracture & fatigue analyses: SGBEM-FEM or XFEM? Part1 1: 2D structures. *CMES - Computer Modeling in Engineering and Sciences*, vol. 90, no. 2, pp. 91–146.

Fantuzzi, N. (2013): *Generalized Differential Quadrature Finite Element Method applied to Advanced Structural Mechanics*. PhD thesis, University of Bologna, 2013.

Ferreira, A. J. M.; Viola, E.; Tornabene, F.; Fantuzzi, N.; Zenkour, A. M. (2013): Analysis of sandwich plates by generalized differential quadrature method. *Mathematical Problems in Engineering*, vol. 2013, pp. 1–12. Article ID 964367, doi:10.1155/2013/964367.

Ferretti, E. (2001): *Modellazione del Comportamento del Cilindro Fasciato in Compressione*. PhD thesis, Università del Salento, 2001.

Ferretti, E. (2003): Crack propagation modeling by remeshing using the Cell Method (CM). *CMES: Computer Modeling in Engineering & Sciences*, vol. 4, pp. 51–72.

Ferretti, E. (2004): A Cell Method (CM) code for modeling the pullout test step-wise. *CMES: Computer Modeling in Engineering & Sciences*, vol. 6, pp. 453–476.

Ferretti, E. (2004): Crack-path analysis for brittle and non-brittle cracks: A Cell Method approach. *CMES: Computer Modeling in Engineering & Sciences*, vol. 6, pp. 227–244.

Ferretti, E. (2004): A discrete nonlocal formulation using local constitutive laws. *International Journal of Fracture*, vol. 130, no. 3, pp. L175–L182.

Ferretti, E. (2005): A local strictly nondecreasing material law for modeling softening and size-effect: a discrete approach. *CMES: Computer Modeling in Engineering & Sciences*, vol. 9, pp. 19–48.

Ferretti, E. (2009): Cell Method analysis of crack propagation in tensioned concrete plates. *CMES: Computer Modeling in Engineering & Sciences*, vol. 54, pp. 253–281.

Ferretti, E. (2012): Shape-effect in the effective law of plain and rubberized concrete. *CMC: Computers, Materials, & Continua*, vol. 30, pp. 237–284.

Ferretti, E. (2013): The Cell Method: an enriched description of physics starting from the algebraic formulation. *CMC: Computers, Materials, & Continua*, vol. 36, no. 1, pp. 49–72.

Ferretti, E. (2013): A Cell Method stress analysis in thin floor tiles subjected to temperature variation. *CMC: Computers, Materials, & Continua*, vol. 36, no. 3, pp. 293–322.

Ferretti, E. (2014): *The Cell Method: a purely algebraic computational method in physics and engineering science*. Momentum Press.

Ferretti, E.; Casadio, E.; Di Leo, A. (2008): Masonry walls under shear test: a CM modeling. *CMES: Computer Modeling in Engineering & Sciences*, vol. 30, pp. 163–190.

Gupta, K. K. (1978): Development of a finite dynamic element for free vibration analysis of two-dimensional structures. *International Journal for Numerical Methods in Engineering*, vol. 12, no. 8, pp. 1311–1327.

Hamidi, M.; Hashemi, M.; Talebbeydokhti, N.; Neill, S. (2012): Numerical modelling of the mild slope equation using localised differential quadrature method. *Ocean Engineering*, vol. 47, pp. 88–103.

Han, Z. D.; Liu, H. T.; Rajendran, A. M.; Atluri, S. N. (2006): The applications of Meshless Local Petrov-Galerkin (MLPG) approaches in high-speed impact, penetration and perforation problems. *CMES - Computer Modeling in Engineering and Sciences*, vol. 14, no. 2, pp. 119–128.

Huang, C.; Leissa, A. (2009): Vibration analysis of rectangular plates with side cracks via the Ritz method. *Journal of Sound and Vibration*, vol. 323, no. 3-5, pp. 974–988.

Huang, C.; Leissa, A.; Chan, C. (2011): Vibrations of rectangular plates with internal cracks or slits. *International Journal of Mechanical Sciences*, vol. 53, no. 6, pp. 436–445.

Huang, C.; Leissa, A.; Li, R. (2011): Accurate vibration analysis of thick, cracked rectangular plates. *Journal of Sound and Vibration*, vol. 330, no. 9, pp. 2079–2093.

Huang, C.; Leissa, A.; Liao, S. (2008): Vibration analysis of rectangular plates with edge v-notches. *International Journal of Mechanical Sciences*, vol. 50, no. 8, pp. 1255–1262.

Lam, K.; Zhang, J.; Zong, Z. (2004): A numerical study of wave propagation in a poroelastic medium by use of localized differential quadrature method. *Applied Mathematical Modelling*, vol. 28, no. 5, pp. 487–511.

Lam, S. (1993): Application of the differential quadrature method to two-dimensional problems with arbitrary geometry. *Computers & Structures*, vol. 47, no. 3, pp. 459–464.

Li, Q.; Shen, S.; Han, Z. D.; Atluri, S. N. (2003): Application of Meshless Local Petrov-Galerkin (MLPG) to problems with singularities, and material discontinuities, in 3-D elasticity. *CMES - Computer Modeling in Engineering and Sciences*, vol. 4, no. 5, pp. 571–585.

Li, S.; Atluri, S. N. (2008): The MLPG mixed collocation method for material orientation and topology optimization of anisotropic solids and structures. *CMES - Computer Modeling in Engineering and Sciences*, vol. 30, no. 1, pp. 37–56.

Li, S.; Atluri, S. N. (2008): Topology-optimization of structures based on the MLPG mixed collocation method. *CMES - Computer Modeling in Engineering and Sciences*, vol. 26, no. 1, pp. 61–74.

Li, Y.; Fantuzzi, N.; Tornabene, F. (2013): On mixed mode crack initiation and direction in shafts: Strain energy density factor and maximum tangential stress criteria. *Engineering Fracture Mechanics*, vol. 109, pp. 273 – 289.

Li, Y.; Viola, E. (2013): Size effect investigation of a central interface crack between two bonded dissimilar materials. *Composite Structures*, vol. 105, pp. 90–107.

Liu, F.-L. (1999): Differential quadrature element method for static analysis of shear deformable cross-ply laminates. *International Journal for Numerical Methods in Engineering*, vol. 46, no. 8, pp. 1203–1219.

Marzani, A.; Tornabene, F.; Viola, E. (2008): Nonconservative stability problems via generalized differential quadrature method. *Journal of Sound & Vibration*, vol. 315, no. 1-2, pp. 176–196.

Nassar, M.; Matbuly, M. S.; Ragb, O. (2013): Vibration analysis of structural elements using differential quadrature method. *Journal of Advanced Research*, vol. 4, no. 1, pp. 93–102.

Nobile, L.; Piva, A.; Viola, E. (2004): On the inclined crack problem in an orthotropic medium under biaxial loading. *Engineering Fracture Mechanics*, vol. 71, no. 4, pp. 529–546.

Pu, S. L.; Hussain, M. A.; Lorensen, W. E. (1978): The collapsed cubic isoparametric element as a ingular element for crack probblems. *International Journal for Numerical Methods in Engineering*, vol. 12, no. 11, pp. 1727–1742.

Ricci, P.; Viola, E. (2006): Stress intensity factors for cracked T-sections and dynamic behaviour of T-beams. *Engineering Fracture Mechanics*, vol. 73, no. 1, pp. 91–111.

Shen, L. H.; Young, D. L.; Lo, D. C.; Sun, C. P. (2009): Local differential quadrature method for 2-D flow and forced-convection problems in irregular domains. *Numerical Heat Transfer, Part B: Fundamentals*, vol. 55, no. 2, pp. 116–134.

Shu, C. (2000): *Differential quadrature and its applications in engineering*. Springer Verlag.

Shu, C.; Chen, W.; Du, H. (2000): Free vibration analysis of curvilinear quadrilateral plates by the differential quadrature method. *Journal of Computational Physics*, vol. 163, no. 2, pp. 452–466.

Sladek, J.; Sladek, V.; Atluri, S. N. (2004): Meshless Local Petrov-Galerkin method for heat conduction problem in an anisotropic medium. *CMES - Computer Modeling in Engineering and Sciences*, vol. 6, no. 3, pp. 309–318.

Sun, J.-A.; Zhu, Z.-Y. (2000): Upwind local differential quadrature method for solving incompressible viscous flow. *Computer Methods in Applied Mechanics and Engineering*, vol. 188, no. 1-3, pp. 495–504.

Timoshenko, S. (1934): *Theory of Elasticity*. Engineering Societies Monographs. McGraw-Hill book Company, Incorporated.

Tonti, E. (2001): A direct discrete formulation of field laws: the Cell Method. *CMES: Computer Modeling in Engineering & Sciences*, vol. 2, pp. 237–258.

Tornabene, F. (2009): Free vibration analysis of functionally graded conical, cylindrical and annular shell structures with a four-parameter power-law distribution. *Computer Methods in Applied Mechanics and Engineering*, vol. 198, no. 37-40, pp. 2911–2935.

Tornabene, F. (2011): 2-D GDQ solution for free vibrations of anisotropic doubly-curved shells and panels of revolution. *Composite Structures*, vol. 93, pp. 1854–1876.

Tornabene, F. (2011): Free vibration of laminated composite doubly-curved shells and panels of revolution via GDQ method. *Computer Methods in Applied Mechanics and Engineering*, vol. 200, pp. 931–952.

Tornabene, F. (2011): Free vibrations of anisotropic doubly-curved shells and panels of revolution with a free-form meridian resting on Winkler-Pasternak elastic foundations. *Composite Structures*, vol. 94, pp. 186–206.

Tornabene, F. (2012): *Meccanica delle strutture a guscio in materiale composito. Il metodo generalizzato di quadratura differenziale*. Esculapio.

Tornabene, F.; Ceruti, A. (2013): Free-form laminated doubly-curved shells and panels of revolution on Winkler-Pasternak elastic foundations: A 2D GDQ solution for static and free vibration analysis. *World Journal of Mechanics*, vol. 3, pp. 1–25.

Tornabene, F.; Ceruti, A. (2013): Mixed static and dynamic optimizazion of four-parameter functionally graded completely doubly-curved and degenerate shells and panels using GDQ method. *Mathematical Problems in Engineering*, vol. 2013, pp. 1–33. Article ID 867079, http://dx.doi.org/10.1155/2013/867079.

Tornabene, F.; Fantuzzi, N.; Viola, E.; Carrera, E. (2014): Static analysis of doubly-curved anisotropic shells and panels using CUF approach, differential geometry and differential quadrature method. *Composite Structures*, vol. 107, pp. 675–697.

Tornabene, F.; Fantuzzi, N.; Viola, E.; Cinefra, M.; Carrera, E.; Ferreira, A.; Zenkour, A. (2014): Analysis of thick isotropic and cross-ply laminated plates by generalized differential quadrature method and a unified formulation. *Composite Part B Engineering*. In Press.

Tornabene, F.; Fantuzzi, N.; Viola, E.; Ferreira, A. J. M. (2013): Radial basis function method applied to doubly-curved laminated composite shells and panels with a general higher-order equivalent single layer theory. *Composite Part B Engineering*, vol. 55, pp. 642–659.

Tornabene, F.; Fantuzzi, N.; Viola, E.; Reddy, J. (2014): Winkler-Pasternak foundation effect on the static and dynamic analyses of laminated doubly-curved and degenerate shells and panels. *Composite Part B Engineering*, vol. 57, pp. 269–296.

Tornabene, F.; Liverani, A.; Caligiana, G. (2011): FGM and laminated doubly-curved shells and panels of revolution with a free-form meridian: a 2-D GDQ solution for free vibrations. *International Journal of Mechanical Sciences*, vol. 53, pp. 446–470.

Tornabene, F.; Liverani, A.; Caligiana, G. (2012): General anisotropic doubly-curved shell theory: a differential quadrature solution for free vibrations of shells and panels of revolution with a free-form meridian. *Journal of Sound & Vibration*, vol. 331, pp. 4848–4869.

Tornabene, F.; Liverani, A.; Caligiana, G. (2012): Laminated composite rectangular and annular plates: A GDQ solution for static analysis with a posteriori shear and normal stress recovery. *Composites Part B Engineering*, vol. 43, pp. 1847–1872.

Tornabene, F.; Liverani, A.; Caligiana, G. (2012): Static analysis of laminated composite curved shells and panels of revolution with a posteriori shear and normal

stress recovery using generalized differential quadrature method. *International Journal of Mechanical Sciences*, vol. 61, pp. 71–87.

Tornabene, F.; Marzani, A.; Viola, E.; Elishakoff, I. (2010): Critical flow speeds of pipes conveying fluid by the generalized differential quadrature method. *Advances in Theoretical and Applied Mechanics*, vol. 3, no. 3, pp. 121–138.

Tornabene, F.; Reddy, J. (2013): FGM and laminated doubly-curved and degenerate shells resting on nonlinear elastic foundation: a GDQ solution for static analysis with a posteriori stress and strain recovery. *Journal of Indian Institute of Science*, vol. 93, no. 4. In Press.

Tornabene, F.; Viola, E. (2007): Vibration analysis of spherical structural elements using the GDQ method. *Computers & Mathematics with Applications*, vol. 53, no. 10, pp. 1538–1560.

Tornabene, F.; Viola, E. (2008): 2-D solution for free vibrations of parabolic shells using generalized differential quadrature method. *European Journal of Mechanics - A/Solids*, vol. 27, no. 6, pp. 1001–1025.

Tornabene, F.; Viola, E. (2009): Free vibration analysis of functionally graded panels and shells of revolution. *Meccanica*, vol. 44, no. 3, pp. 255–281.

Tornabene, F.; Viola, E. (2009): Free vibrations of four-parameter functionally graded parabolic panels and shell of revolution. *European Journal of Mechanics - A/Solids*, vol. 28, no. 5, pp. 991–1013.

Tornabene, F.; Viola, E. (2013): Static analysis of functionally graded doubly-curved shells and panels of revolution. *Meccanica*, vol. 48, pp. 901–930.

Tornabene, F.; Viola, E.; Fantuzzi, N. (2013): General higher-order equivalent single layer theory for free vibrations of doubly-curved laminated composite shells and panels. *Composite Structures*, vol. 104, pp. 94–117.

Tornabene, F.; Viola, E.; Inman, D. (2009): 2-D differential quadrature solution for vibration analysis of functionally graded conical, cylindrical and annular shell structures. *Journal of Sound & Vibration*, vol. 328, no. 3, pp. 259–290.

Tsai, C.; Young, D.; Hsiang, C. (2011): The localized differential quadrature method for two-dimensional stream function formulation of navier-stokes equations. *Engineering Analysis with Boundary Elements*, vol. 35, no. 11, pp. 1190–1203.

Viola, E.; Artioli, E.; Dilena, M. (2005): Analytical and differential quadrature results for vibration analysis of damaged circular arches. *Journal of Sound and Vibration*, vol. 288, no. 4-5, pp. 887–906.

Viola, E.; Dilena, M.; Tornabene, F. (2007): Analytical and numerical results for vibration analysis of multi-stepped and multi-damaged circular arches. *Journal of Sound & Vibration*, vol. 299, no. 1-2, pp. 143–163.

Viola, E.; Fantuzzi, N.; Marzani, A. (2012): Cracks interaction effect on the dynamic stability of beams under conservative and nonconservative forces. *Key Engineering Materials*, vol. 488-489, pp. 383–386.

Viola, E.; Li, Y.; Fantuzzi, N. (2012): On the stress intensity factors of cracked beams for structural analysis. *Key Engineering Materials*, vol. 488-489, pp. 379–382.

Viola, E.; Marzani, A. (2004): Crack effect on dynamic stability of beams under conservative and nonconservative forces. *Engineering Fracture Mechanics*, vol. 71, no. 4-6, pp. 699–718.

Viola, E.; Nobile, L.; Federici, L. (2002): Formulation of cracked beam element for structural analysis. *Journal of Engineering Mechanics*, vol. 128, no. 2, pp. 220–230.

Viola, E.; Ricci, P.; Aliabadi, M. (2007): Free vibration analysis of axially loaded cracked timoshenko beam structures using the dynamic stiffness method. *Journal of Sound and Vibration*, vol. 304, no. 1-2, pp. 124–153.

Viola, E.; Rossetti, L.; Fantuzzi, N. (2012): Numerical investigation of functionally graded cylindrical shells and panels using the generalized unconstrained third order theory coupled with the stress recovery. *Composite Structures*, vol. 94, pp. 3736–3758.

Viola, E.; Tornabene, F. (2005): Vibration analysis of damaged circular arches with varying cross-section. *Structural Integrity & Durability (SID-SDHM)*, vol. 1, no. 2, pp. 155–169.

Viola, E.; Tornabene, F. (2006): Vibration analysis of conical shell structures using GDQ method. *Far East Journal of Applied Mathematics*, vol. 25, no. 1, pp. 23–39.

Viola, E.; Tornabene, F. (2009): Free vibrations of three parameter functionally graded parabolic panels of revolution. *Mechanics Research Communications*, vol. 36, no. 5, pp. 587–594.

Viola, E.; Tornabene, F.; Fantuzzi, N. (2013): General higher-order shear deformation theories for the free vibration analysis of completely doubly-curved laminated shells and panels. *Composite Structures*, vol. 95, pp. 639–666.

Viola, E.; Tornabene, F.; Fantuzzi, N. (2013): Generalized differential quadrature finite element method for cracked composite structures of arbitrary shape. *Composite Structures*, vol. 106, pp. 815–834.

Viola, E.; Tornabene, F.; Fantuzzi, N. (2013): Static analysis of completely doubly-curved laminated shells and panels using general higher-order shear deformation theories. *Composite Structures*, vol. 101, pp. 59–93.

Wang, T.; Cao, S.; Ge, Y. (2013): Generation of inflow turbulence using the local differential quadrature method. *Journal of Wind Engineering and Industrial Aerodynamics*. In press.

Wang, X.; Wang, Y.-L.; Chen, R.-B. (1998): Static and free vibrational analysis of rectangular plates by the differential quadrature element method. *Communications in Numerical Methods in Engineering*, vol. 14, no. 12, pp. 1133–1141.

Wang, Y.; Wang, X.; Zhou, Y. (2004): Static and free vibration analyses of rectangular plates by the new version of the differential quadrature element method. *International Journal for Numerical Methods in Engineering*, vol. 59, no. 9, pp. 1207–1226.

Xing, Y.; Liu, B. (2009): High-accuracy differential quadrature finite element method and its application to free vibrations of thin plate with curvilinear domain. *International Journal for Numerical Methods in Engineering*, vol. 80, no. 13, pp. 1718–1742.

Xing, Y.; Liu, B.; Liu, G. (2010): A differential quadrature finite element method. *International Journal of Applied Mechanics*, vol. 2, pp. 207–227.

Yilmaz, Y.; Girgin, Z.; Evran, S. (2013): Buckling analyses of axially functionally graded nonuniform columns with elastic restraint using a localized differential quadrature method. *Mathematical Problems in Engineering*, vol. 2013, pp. 1–12. Article ID 793062, http://doi:10.1155/2013/793062.

Zhao, C.; Steven, G. (1996): Asymptotic solutions for predicted natural frequencies of two-dimensional elastic solid vibration problems in finite element analysis. *International Journal for Numerical Methods in Engineering*, vol. 39, no. 16, pp. 2821–2835.

Zhong, H.; He, Y. (1998): Solution of poisson and laplace equations by quadrilateral quadrature element. *International Journal of Solids and Structures*, vol. 35, no. 21, pp. 2805–2819.

Zhong, H.; Yu, T. (2009): A weak form quadrature element method for plane elasticity problems. *Applied Mathematical Modelling*, vol. 33, no. 10, pp. 3801–3814.

Zong, Z.; Lam, K. (2002): A localized differential quadrature (LDQ) method and its application to the 2D wave equation. *Computational Mechanics*, vol. 29, no. 4-5, pp. 382–391.

Zong, Z.; Zhang, Y. (2009): *Advanced differential quadrature methods*. Chapman & Hall/CRC Applied Mathematics & Nonlinear Science. Taylor & Francis.